Quantum optical diode with semiconductor microcavities

H. Z. Shen,[1] Y. H. Zhou,[1] and X. X. Yi[2,*]

[1]*School of Physics and Optoelectronic Technology, Dalian University of Technology, Dalian 116024, China*

[2]*Center for Quantum Sciences and School of Physics, Northeast Normal University, Changchun 130024, China*

(Received 27 May 2014; published 26 August 2014)

The semiconductor diode, which acts as an electrical rectifier and allows unidirectional electronic transports, is the key to information processing in integrated circuits. Analogously, an optical rectifier (or diode) working at specific target wavelengths has recently become a highly sought-after device in optical communication and signal processing. In this paper, we propose a scheme to realize an optical diode for photonic transport at the level of few photons. The system consists of two spatially overlapping single-mode semiconductor microcavities coupled via $\chi^{(2)}$ nonlinearities. The photon blockade is predicted to take place in this system. These photon blockade effects can be achieved by tuning the frequency of the input laser field (driving field). Based on those blockades, we analytically derive the one- and two-photon current in terms of a zero and a finite time-delayed two-order correlation function. The results suggest that the system can serve as a one- and two-photon quantum optical diode which allows transmission of photons in one direction much more efficiently than in the other.

DOI: 10.1103/PhysRevA.90.023849 PACS number(s): 42.50.Pq, 42.50.Ct, 73.40.Ei, 78.66.Fd

I. INTRODUCTION

The electrical diode is a two-terminal electronic device with asymmetric conductance. It has low resistance to current flow in one direction and high resistance in the opposite direction. The study of electrical diodes can be traced back to more than a century ago, when the first device enabled the rectification of current flux. Motivated by the significant rectifying capabilities of electric diodes, considerable efforts have been made to investigate the rectification of other energy forms, for example, thermal flux [1–6] and solitary waves [7].

Efforts have also been made to investigate the optical diodes. Optical diodes, also known as optical isolators [8], are an optical rectifier working at specific target wavelengths. They allow propagation of a photon signal in one direction and block that in the opposite direction. Motivated by potential applications in a quantum network of light, various possible solid-state optical diodes have been proposed, including the diodes from standard bulk Faraday rotators [9,10], the diodes integrated on a chip [11–15], and diodes operating in an optically controllable way [11,16,17], as well as the diodes at low-field intensities or even at the single-photon levels [18].

The physics behind the optical diode is the breaking of time-reversal symmetry, which is typically achieved via acoustic rectifiers [19,20], moving photonic crystal [21], spin-photon entangling [22], and few-photon tunneling [23–25]. Thanks to the classical level at which these schemes work, they have now been attained in different configurations on-chip [13,14,26].

With the recent advances in quantum photonic technologies at the single-photon levels [27], researchers have made a step further in the study of the optical diode, i.e., the *quantum optical diode*. Tunable one- or two-photon quantum rectification is likely to play an important role in this case, analogous to the classical electrical diodes in current microchips. A quantum optical rectifier is a two-terminal, spatially nonreciprocal device that allows unidirectional propagation of single or few quanta of (electromagnetic) energy at a fixed signal frequency and amplitude [28]. Up to now, only a few proposals have been made [18,28] in the fully quantum regime.

In this paper, we propose a fully quantum diode with two coupled semiconductor microcavities driven by external fields. The merit of this proposal is to unify the unidirectional transport of photon and photon conversion. The system consists of two spatially overlapping single-mode cavities with frequencies ω_b and ω_a, respectively. The two cavities are coupled by $\chi^{(2)}$ nonlinearities that mediate the conversion of a photon in cavity b to two photons in cavity a, and vice versa [29–33]. The physics behind this proposal is the photon blockade. When cavity a is pumped, the single-photon blockade prevails in the system; the single photon that occupies the Fock state first blockades the generation of more photons. When the pumping is on cavity b, due to the existence of the two-photon eigenstate of the system, a two-photon blockade dominates, blockading more photons in cavity b.

The single-photon blockade was already observed in standard cavity quantum electrodynamics (QED) [34–43], optomechanical systems [44–47], and in a circuit QED system [48,49]. The proposal presented here is to use these techniques and show the one- and two-photon blockade effect by changing the intensity and frequency of the driving field.

To be specific, we present a proposal for an optical diode in microcavities. By analyzing the propagation of photons in the system, we observe a significant rectifying effect that allows the photons with a fixed frequency to propagate in one direction but suppresses them in the opposite direction. Based on the analysis of the underlying rectifying mechanism and detailed examination of the parameter dependence of the rectifying efficiency, we find that the system may be identified as a diode in a wide range of parameters despite its simplicity.

The remainder of the paper is organized as follows. In Sec. II, we introduce the system and present a model to describe the system. The one- and two-photon blockades are predicted and discussed. In Sec. III, in terms of the two-order correlation function and photon number statistics, we analyze a specific one-photon and two-photon diode. In Sec. IV, we investigate the rectification of the diode via two-time correlation functions. Section V is devoted to the experimental

*Corresponding author: yixx@nenu.edu.cn

realization of a few-photon optical diode. Discussion and conclusions are given in Sec. VI.

II. MODEL AND PHOTON BLOCKADE

Throughout this work, we adopt the International System (SI) of units [50]. The nonlinear optical response of dielectric material to an electric field is given by

$$D_i(\mathbf{r},t) = \sum_{jkm} \{\varepsilon_0 \varepsilon_{ij}(\mathbf{r}) E_j(\mathbf{r},t) + \varepsilon_0 [\chi^{(2)}_{ijk}(\mathbf{r}) E_j(\mathbf{r},t) E_k(\mathbf{r},t) + \chi^{(3)}_{ijkm}(\mathbf{r}) E_j(\mathbf{r},t) E_k(\mathbf{r},t) E_m(\mathbf{r},t) + \cdots]\}, \quad (1)$$

which defines the relative dielectric permittivity tensor of the medium, $\varepsilon_{ij}(\mathbf{r}) = \delta_{ij} + \chi^{(1)}_{ij}(\mathbf{r})$. We will consider only the nonlinear response up to second order in the electromagnetic field, i.e., we assume $\chi^{(3)}_{ijkm}(\mathbf{r}) = 0$ and only take the optical nonlinear effects caused by $\chi^{(2)}_{ijk}$ in Eq. (1) into account. We assume the material is isotropic, i.e., $\varepsilon_{ij}(\mathbf{r}) \to \varepsilon(\mathbf{r})$ is a spatially dependent scalar quantity. The canonical quantization can be done by expressing the field operators as

$$\hat{E}(\mathbf{r},t) = \sum_{j=a,b} \sqrt{\frac{\hbar\omega_j}{2\epsilon_0}} \left[\hat{h}_j \frac{\vec{\phi}_j(\mathbf{r})}{\sqrt{\varepsilon(\mathbf{r})}} e^{-i\omega_j t} + \text{H.c.} \right], \quad (2)$$

and $\hat{B}(\mathbf{r},t) = -\nabla \times \hat{E}(\mathbf{r},t)/\omega_0$, with H.c. standing for the Hermitian conjugate. Here, $\hat{h}_a = \hat{a}$ and $\hat{h}_b = \hat{b}$ denote the photon destruction operators in the two cavities with frequencies ω_a and $\omega_b = 2\omega_a$, respectively. For each cavity mode, the three-dimensional cavity field $\phi_j(\mathbf{r})$ must be normalized by $\int |\vec{\phi}_j(\mathbf{r})|^2 d^3\mathbf{r} = 1$ $(j = a,b)$. By the energy density formula in classical electrodynamics, $H_{em} = \frac{1}{2}\int [\mathbf{E}(\mathbf{r},t)\mathbf{D}(\mathbf{r},t) + \int \mathbf{H}(\mathbf{r},t)\mathbf{B}(\mathbf{r},t)]d^3\mathbf{r}$, where $\mathbf{H}(\mathbf{r},t) = \mathbf{B}(\mathbf{r},t)/\mu_0$, an interaction Hamiltonian in the second quantization can be obtained [29,31],

$$\hat{H}_0 = \hbar\omega_a \hat{a}^\dagger \hat{a} + \hbar\omega_b \hat{b}^\dagger \hat{b} + \hbar\Omega(\hat{b}^\dagger \hat{a}^2 + \text{H.c.}), \quad (3)$$

where the nonlinear interaction coefficient is defined by

$$\Omega = \sqrt{\frac{\hbar\omega_a^2\omega_b}{2\varepsilon_0}} \sum_{ijk} \int \frac{\chi^{(2)}_{ijk}(\mathbf{r})}{[\varepsilon(\mathbf{r})]^{1.5}} \phi^*_{i,a}(\mathbf{r}) \phi^*_{j,a}(\mathbf{r}) \phi_{k,b}(\mathbf{r}) d^3\mathbf{r}. \quad (4)$$

For the scheme to work, external driving for cavity a or b is essential. We illustrate the setup in Fig. 1(a). The driving frequency is denoted by ω_L for cavity a and $2\omega_L$ for cavity b, respectively. F stands for the driving strength. The corresponding Hamiltonian is

$$\hat{H}_{dr}(t) = \hat{H}_0 + \hbar F \hat{h}_j e^{-i\lambda_j\omega_L t} + \hbar F^* \hat{h}_j^\dagger e^{i\lambda_j\omega_L t}, \quad (5)$$

where $\lambda_a = 1$ and $\lambda_b = 2$. In a rotating frame defined by $\hat{U}_S(t) = \exp[i\omega_L t(\hat{a}^\dagger \hat{a} + 2\hat{b}^\dagger \hat{b})]$, the Hamiltonian is

$$\hat{H}_S = \hbar\Delta_a \hat{a}^\dagger \hat{a} + \hbar\Delta_b \hat{b}^\dagger \hat{b} + \hbar\Omega(\hat{b}^\dagger \hat{a}^2 + \hat{a}^{\dagger 2}\hat{b}) + \hbar F \hat{h}_j + \hbar F^* \hat{h}_j^\dagger, \quad (6)$$

where $\Delta_a = \omega_a - \omega_L$ and $\Delta_b = \omega_b - 2\omega_L$ define the detunings of the cavity a and cavity b modes from the driving laser, respectively.

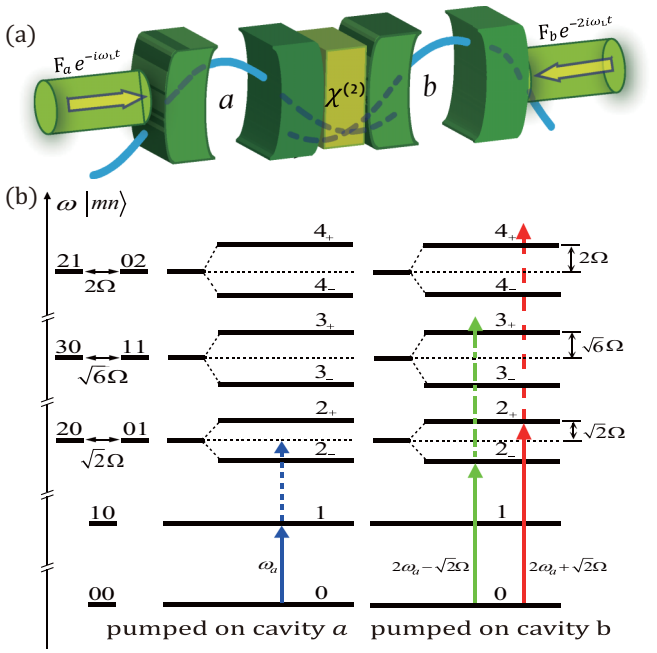

FIG. 1. (Color online) (a) Illustration of the setup. The two cavities driven by external fields (pumping) are coupled by χ^2 nonlinearities. The pumping on the cavity a is resonant with the field inside cavity a, while the pumping on cavity b is at $2\omega_a + \sqrt{2}\Omega$ or $2\omega_a - \sqrt{2}\Omega$. (b) Level diagram for the two coupled cavities with $\omega_b = 2\omega_a$. States are labeled by $|mn\rangle$ with the first (second) number denoting the photon number in cavity a (cavity b). The coupling Ω splits the degeneracy of states $|mn\rangle$ and $|m-2n+1\rangle$ or $|m+2n-1\rangle$. The arrows show the frequency of the driven field.

The nonlinear terms proportional to Ω in Eq. (6) describe coherent photon exchange between the two optical cavity modes. The resulting low-energy level diagram is shown in Fig. 1(b), where $|mn\rangle$ as before represents the state with m and n photons in the cavity a and b, respectively. In the absence of driving fields, we diagonalize $\hat{H}_S$ with $\omega_b = 2\omega_a$ and $\omega_L = \omega_a$. The ground state and low excited state are

$$\begin{aligned} |0\rangle &= |00\rangle, \\ |1\rangle &= |10\rangle, \\ |2_\pm\rangle &= \frac{1}{\sqrt{2}} |01\rangle \pm |20\rangle, \\ |3_\pm\rangle &= \frac{1}{\sqrt{2}} |11\rangle \pm |30\rangle, \\ |4_\pm\rangle &= \frac{1}{\sqrt{2}} |02\rangle \pm |21\rangle. \end{aligned} \quad (7)$$

The driving field couples all states which differ from each other by a single photon. In the following sections, we will restrict ourselves to consider a very weak driving field such that the Hilbert space can be truncated to low-energy levels, as listed in Eq. (7).

In addition to the coherent evolution governed by the Hamiltonian $\hat{H}_S$, we introduce cavity losses to the system, and the dynamics of the system is described by

$$\dot{\rho} = -i[\hat{H}_S, \rho] + \kappa_a \mathcal{D}(\hat{a})\rho + \kappa \mathcal{D}(\hat{b})\rho, \quad (8)$$

where $\hat{H}_S$ is given by Eq. (6), κ and κ_a denote loss rates for the two cavities, respectively, and the superoperator $\mathcal{D}(\hat{o}) = \hat{o}\rho\hat{o}^\dagger - \frac{1}{2}\hat{o}^\dagger\hat{o}\rho - \frac{1}{2}\rho\hat{o}^\dagger\hat{o}$. According to the Markovian input-output formalism of Collett and Cardiner [51–53], the input, output, and intracavity fields are linked by the input-output relation,

$$\begin{aligned}\hat{a}_{\rm out}(t) &= \hat{a}_{\rm in}(t) + \sqrt{\kappa_a}\hat{a}(t),\\ \hat{b}_{\rm out}(t) &= \hat{b}_{\rm in}(t) + \sqrt{\kappa}\hat{b}(t).\end{aligned} \tag{9}$$

For an arbitrary state of the input modes, correlations of the output fields would depend on cross correlations between the input and intracavity fields, which in turn would require one to model the input fields together with the system dynamics. However, if we assume that only classical driving fields are added to the quantum vacuum of the input-output channels, then all normally ordered cross correlations between intracavity and input modes vanish, and correlations in the output channels can be expressed as functions of intracavity correlations only. With this assumption, the average output current (or photon stream) at time t can be formally given by

$$N_j(t) = \kappa_j {\rm Tr}[\hat{h}_j^\dagger \hat{h}_j \rho(t)]. \tag{10}$$

We will set $\kappa_b \equiv \kappa$ hereafter.

Now we discuss the photon-blockade effect. This effect can be characterized by the second-order correlation function with no time delay [54,55],

$$g_j^{(2)}(0) = \frac{\langle \hat{h}_j^{\dagger 2}\hat{h}_j^2\rangle}{\langle \hat{h}_j^\dagger \hat{h}_j\rangle^2}, \tag{11}$$

where all operators are evaluated at the same instance of time. In Fig. 2, we show $g_a^{(2)}(0)$ and $g_b^{(2)}(0)$ as a function of detuning. The figures are plotted in the weak driving limit. Interesting features can been found at detunings $0, -\frac{1}{\sqrt{2}}, \frac{1}{\sqrt{2}}, -\sqrt{2}, \sqrt{2}$, and 0 marked, respectively, by A–F. Recalling that $g_j^{(2)}(0) < 1$ indicates photon antibunching and $g_j^{(2)}(0) \to 0$ implies complete photon blockade, we find that point A exactly corresponds to the single-photon blockade, similar to that in Kerr-type [35,54,56] or QED [34–40] nonlinear systems. Remarkably, when cavity b is pumped, a two-photon blockade for cavity a occurs. This can be found at points D and E in Fig. 2(c). Of course, for cavity b, it is still a single-photon blockade. We refer to this effect as the two-photon blockade from the aspect of cavity a, which means that the two-photon Fock states blockade the generation of more photons.

To gain more insight into the one- and two-photon blockade shown in Fig. 2, we develop an approximately analytic expression for the system by considering only the eight lowest energy levels in Fig. 1(b). By assuming that the system is initially prepared in $|00\rangle$ and only these levels are occupied due to the pumping of the driving, the state of the system can be written as [57]

$$\begin{aligned}|\Phi\rangle = {} & C_{00}|00\rangle + C_{10}|10\rangle + C_{01}|01\rangle + C_{20}|20\rangle\\ & + C_{11}|11\rangle + C_{30}|30\rangle + C_{21}|21\rangle + C_{02}|02\rangle,\end{aligned} \tag{12}$$

and we take the effective Hamiltonian $\hat{H}_{\rm eff} = \hat{H}_S - i[\kappa_a\hat{a}^\dagger\hat{a} + \kappa\hat{b}^\dagger\hat{b}]/2$ to describe the system. This approach allows us to

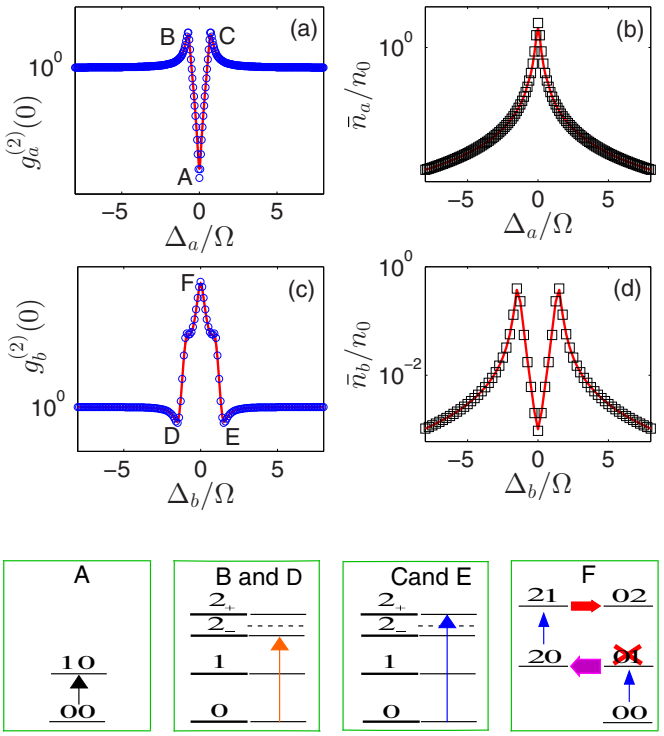

FIG. 2. (Color online) Rescaled average photon number (black squares) and the equal-time second-order correlation function (blue circles) as a function of detunings. *The photon number is rescaled by F^2 to fit the correlation function.* (a) and (b) are for the case with cavity a pumped, and (c) and (d) for cavity b pumped. Once one cavity is pumped, another is left free. Dotted lines are analytical results [see Eqs. (14)–(17)]. Red solid lines show the numerical results. *Here and hereafter, Ω, F, Δ_a, Δ_b, and κ_a are rescaled in units of κ, and t is then in units of $1/\kappa$. Hence all parameters are dimensionless.* In all plots, we chose $\Omega/\kappa = 4$, $F/\kappa = 0.2$, $\omega_a/\kappa = 1$, $\omega_b/\kappa = 2$, and $\kappa_a/\kappa = 1$. A–F mark the maximum and minimum, where the corresponding detunings are A: $\Delta_a/\Omega = 0$; B: $-\frac{1}{\sqrt{2}}$; C: $\frac{1}{\sqrt{2}}$; D: $\Delta_b/\Omega = -\sqrt{2}$; E: $\sqrt{2}$; and F: 0. The tiny deviation of the analytical results from the numerical ones is caused by the approximation $F/\kappa \ll 1$ used in Eqs. (14)–(17). A–F in the bottom panels illustrate the transitions that may lead to the features seen at the points A–F. Suppression of the steady-state population of the level $|01\rangle$ is indicated by a red X. Further explanation of the features can be found in the main text.

evaluate the mean occupation numbers up to the order of F^2 and the second-order correlation function up to the order of F^4. By substituting $|\Phi\rangle$ into the Schrödinger equation $i\partial_t|\Phi\rangle = \hat{H}_{\rm eff}|\Phi\rangle$ ($\hbar = 1$, hereafter), we find the following coupled equations:

$$\begin{aligned}\dot{C}_{00} &= 0,\\ \dot{C}_{10} &= -iFC_{11} - \delta_a C_{10},\\ \dot{C}_{20} &= -i\sqrt{2}\Omega C_{01} - 2\delta_a C_{20},\\ \dot{C}_{01} &= -i\sqrt{2}\Omega C_{20} - iFC_{00} - \delta_b C_{01},\\ \dot{C}_{11} &= -i\sqrt{6}\Omega C_{30} - iFC_{10} - (\delta_a+\delta_b)C_{11},\\ \dot{C}_{30} &= -i\sqrt{6}\Omega C_{11} - 3\delta_a C_{30},\\ \dot{C}_{21} &= -i2\Omega C_{02} - iFC_{20} - (2\delta_a+\delta_b)C_{21},\\ \dot{C}_{02} &= -i2\Omega C_{21} - i\sqrt{2}FC_{01} - 2\delta_b C_{02},\end{aligned} \tag{13}$$

where $\delta_j = \kappa_j/2 + \Delta_j i$, and cavity b being pumped is assumed. At steady states, these amplitudes C_{ij} do not evolve. The mean occupation numbers in this case are $\bar{n}_a = 2|\bar{C}_{20}|^2$ and $\bar{n}_b = |\bar{C}_{01}|^2$, where $\bar{C}_{ij}$ denote the amplitude at the steady state. Up to first order in F/κ (see Appendix A), the mean photon number is

$$\begin{aligned}\frac{\bar{n}_a}{n_0} &= \frac{2\Omega^2}{S\left(\frac{1}{4},-\Delta_b,1,\frac{\Delta_b}{2},\frac{1}{2}\right)},\\ \frac{\bar{n}_b}{n_0} &= \frac{4S\,(1,0,0,0,2)}{S\,(1,-4\Delta_b,4,2\Delta_b,2)},\end{aligned} \tag{14}$$

where $S\,(a,b,c,d,e) = (a\kappa_a + b\Delta_a + c\Omega^2)^2 + (d\kappa_a + e\Delta_a)^2$ and $n_0 = (F/\kappa)^2$. From $S\,(a,b,c,d,e)$ in these equations, we can obtain the location for local maxima and minima of the average photon numbers, which are in excellent agreement with the numerical results shown in Fig. 2. The eight-level model also provides us with the analytical expression of the second-order correlation functions (see Appendix A),

$$\begin{aligned}g_a^{(2)}(0) &= \frac{S\left(\frac{1}{4},-\Delta_b,1,\frac{\Delta_b}{2},\frac{1}{2}\right)}{4F^2\Omega^2},\\ g_b^{(2)}(0) &= \frac{S\left(-\frac{1}{2}a_0,2\Delta_a+\Delta_b,1,2\Delta_a+\frac{1}{2}\Delta_b,\frac{1}{2}\right)}{S\left(-\frac{1}{2},2\Delta_b,-2+\frac{-1+4\Delta_b^2}{4\Omega^2},\Delta_b,1+\frac{\Delta_b}{\Delta_a}\right)}\\ &\quad\times\frac{S\,(1,-4\Delta_b,4,2\Delta_b,2)}{S^2\,(1,0,0,0,2)},\end{aligned} \tag{15}$$

where $a_0 = \kappa_a + 1/2$. Using the same approach, we can obtain the following equations for the case of cavity a being pumped:

$$\begin{aligned}\dot{C}_{00} &= 0,\\ \dot{C}_{10} &= -iFC_{00} - i\sqrt{2}FC_{20} - \delta_a C_{10},\\ \dot{C}_{20} &= -i\sqrt{2}\Omega C_{01} - 2\delta_a C_{20} - i\sqrt{2}FC_{10},\\ \dot{C}_{01} &= -i\sqrt{2}\Omega C_{20} - \delta_b C_{01},\\ \dot{C}_{11} &= -i\sqrt{6}\Omega C_{30} - iFC_{01} - i\sqrt{2}FC_{21} - (\delta_a+\delta_b)C_{11},\\ \dot{C}_{30} &= -i\sqrt{6}\Omega C_{11} - 3\delta_a C_{30} - i\sqrt{3}FC_{20},\\ \dot{C}_{21} &= -i2\Omega C_{02} - i\sqrt{2}FC_{11} - (2\delta_a+\delta_b)C_{21},\\ \dot{C}_{02} &= -i2\Omega C_{21} - 2\delta_b C_{02}.\end{aligned} \tag{16}$$

The steady-state amplitudes (see Appendix A) are given by

$$\begin{aligned}\frac{\bar{n}_a}{n_0} &= \frac{4}{S\,(1,0,0,0,2)},\\ \frac{\bar{n}_b}{n_0} &= \frac{(F\Omega)^2}{S\left(\frac{1}{2},0,0,0,1\right)S\left(\frac{1}{4},-\Delta_b,1,\frac{\Delta_b}{2},\frac{1}{2}\right)},\\ g_a^{(2)}(0) &= \frac{S\,(1,0,0,0,2)\,S\left(\frac{1}{\kappa_a},0,0,\frac{2\Delta_b}{\kappa_a},0\right)}{S\,(1,-4\Delta_b,4,2\Delta_b,2)},\\ g_b^{(2)}(0) &= \frac{S\,(1,0,0,0,2)\,S\left(\frac{1}{4},-\Delta_b,1,\frac{\Delta_b}{2},\frac{1}{2}\right)}{S\,(a_1,b_1,c_1,d_1,e_1)\,S^{-1}\left(\frac{\Delta_b}{\kappa_a},1,0,\frac{1}{2},\frac{1}{2\Delta_a}\right)},\end{aligned} \tag{17}$$

where

$$\begin{aligned}a_1 &= -\frac{1}{16} - \frac{3\kappa_a}{16} - \frac{\kappa_a^2}{8} + \frac{3\Delta_b^2}{4} + \frac{3\kappa_a\Delta_b^2}{4},\\ b_1 &= \frac{3\Delta_a}{4} + \frac{3\kappa_a\Delta_a}{2} - 3\Delta_a\Delta_b^2 - \Delta_b^3 + \Delta_b f_1,\\ c_1 &= -\frac{1}{2} - \frac{3\kappa_a}{2} - \frac{\kappa_a^2}{2} + 2\Delta_a^2 + 2\Delta_b^2 - 4\Omega^2,\\ d_1 &= -\frac{3\Delta_a}{4} - 3\Delta_b\Omega^2 - \frac{3}{4}\kappa_a\Delta_a + \frac{\Delta_b^3}{2} + \Delta_b g_1,\\ e_1 &= -\frac{1}{8} + \Delta_a^2 + 3\Delta_a\Delta_b + \frac{3}{2}\Delta_b^2 + \Omega^2 h_1.\end{aligned} \tag{18}$$

Here, $f_1 = \frac{3}{4} + 3\kappa_a + \frac{3\kappa_a^2}{2} - 2\Delta_a^2 + 6\Omega^2$, $g_1 = -\frac{3}{8} - \frac{3}{4}\kappa_a - \frac{1}{4}\kappa_a^2 + 3\Delta_a^2 + 3\Delta_a\Delta_b$, and $h_1 = -3 - 2\frac{\Delta_b}{\Delta_a} - 2\kappa_a$. Similarly, by analyzing $S(a,b,c,d,e)$ in Eqs. (14)–(17), we can obtain interesting points in $g_{a,b}^{(2)}(0)$ labeled by A–F, which are in excellent agreement with the numerical results shown in Fig. 2.

We now discuss the features observed in Fig. 2. We will use the eight-level model together with the diagonal basis in Eq. (7) to understand the physics behind the features. In Figs. 2(a) and 2(b), e.g., the pumping is on microcavity a, and when the detuning is zero, $\Delta_a = 0$ (point A in Fig. 2), we can see $g_a^{(2)}(0) \ll 1$, indicating complete antibunching due to the suppressed two-photon process (panel A, bottom of Fig. 2). This leads to the single-photon blockade. Physically, when the left cavity a is pumped by an incident laser of frequency ω_L, an incident photon with the the same frequency as the cavity field ω_a will excite the cavity from vacuum $|0\rangle$ to the first excited state $|1\rangle$ [marked by the blue dotted arrow in Fig. 1(b)]. Once the cavity has a photon, the second photon at that frequency will be blocked because, due to the nonlinearity of (3), excitation of the system from $|1\rangle$ to $|2_+\rangle$ or $|2_-\rangle$ requires an additional energy $\hbar\sqrt{2}\Omega$, which cannot be supplied by the second photon. At the detuning $\Delta_a/g = \pm\frac{1}{\sqrt{2}}$ [points B and C of Fig. 2(a)], bunching happens due to the two-photon resonant transition $|0\rangle \to |2_+\rangle$ and$|2_-\rangle$ (panels B and C, bottom of Fig. 2). The physics behind this bunching is similar.

A similar story takes place when the microcavity b is pumped; see Fig. 2(c). At detuning $\Delta_b/g = \pm\sqrt{2}$ [points D and E of Fig. 2(c)], resonant transition $|0\rangle \to |2_+\rangle$ and $|2_-\rangle$ (panels D and E, bottom of Fig. 2) occurs, indicating almost complete antibunching for cavity mode b. Mathematically, we find that both the one-photon occupation amplitude $\bar{C}_{10}$ and the three-photon occupation amplitudes $\bar{C}_{11}$ and $\bar{C}_{30}$ equal zero, while the two-photon occupation amplitudes $\bar{C}_{01}$ and $\bar{C}_{20}$ are much larger than that of four-photon occupation under the weak driving limit $|\alpha_j\alpha_k| \ll 1$; see Eq. (A1). The point F in Fig. 2 corresponds to detuning $\Delta_b = 0$. At this point, $g_b^{(2)}(0) \gg 1$, indicating strong bunching. This is due to destructive interference that suppresses the population on $|01\rangle$ (panel F, bottom of Fig. 2), steering the system into a dark state, $|\text{dark}\rangle = -\cos\varphi|00\rangle + \sin\varphi\,|20\rangle$, where $\tan\varphi = F/\Omega$. This is reminiscent of the electromagnetically induced transparency [58,59]. Due to the weak coupling, $|20\rangle$ is almost not populated when the system occupies the dark state. This induces the transition from $|20\rangle$ to $|21\rangle$, which in turn is strongly coupled to $|02\rangle$. The net result is the transition

where one photon is suppressed compared to the two-photon transition, leading to the bunching at $\Delta_b = 0$.

To confirm this point, we now show that two-photon resonance is absent at $\Delta_b = 0$. At first glance, the level diagram in Fig. 1(b) together with bunching at point F in Fig. 2 suggest a two-photon resonance at zero detuning $\Delta_b = 0$, where the energy of the two-photon state $|02\rangle$ is equal to the energy of two incident photons in mode b. However, as discussed above, the strong bunching effect at $\Delta_b = 0$ comes completely from the suppression of the one-photon population. Further, we find that the expected two-photon resonance is canceled by interference. This can be seen from a second-order perturbative calculation of the two-photon Rabi frequency $\omega^{(2)}_{00\to 02}$ for the transition $|00\rangle \to |02\rangle$. The two-photon state $|02\rangle$ can be populated by the drive $\hat{h}_{dr} = F(\hat{b} + \hat{b}^\dagger)$ from vacuum via two intermediate one-photon eigenstates $|2_\pm\rangle$ given by Eq. (7) with energies $\omega_{2\pm} = \Delta_b \pm \sqrt{2}\Omega$ in the rotating frame. The resulting Rabi frequency is

$$\omega^{(2)}_{00\to 02} = \sum_{m=2_+,2_-} \langle 20|\hat{h}_{dr}|m\rangle \langle m|\hat{h}_{dr}|00\rangle / \omega_m, \qquad (19)$$

which vanishes at $\Delta_b = 0$ as a consequence of destructive interference between the two amplitudes. Although the exact cancellation is lifted by including finite dissipation and the full spectrum, this simple argument shows that the expected two-photon resonance at $\Delta_b = 0$ is strongly suppressed.

It is important to address that the photon blockade in the case of cavity b being driven is a two-photon blockade from the side of cavity a. Hence we refer to this type of photon blockade as a two-photon blockade.

So far, we have demonstrated both analytically and numerically a variety of quantum properties revealing the unique nature of the one- and two-photon blockade. The results suggest that by manipulating the detuning, optical diodes may be realized in such a system based on the explicit one- and two-photon blockade.

III. ONE-PHOTON AND TWO-PHOTON DIODE

By the use of the blockade features of the photonic semiconductor microcavities and the χ^2 nonlinearities, in this section we present a scheme to realize a one-photon and two-photon diode. We define a rectifying factor as the normalized difference between the two output currents corresponding to the system being pumped through the left and right cavities (indicated by the wave vectors k and $-k$, respectively) [28],

$$R = \frac{2N_b(k) - N_a[-k]}{2N_b(k) + N_a[-k]}. \qquad (20)$$

Substituting Eqs. (14)–(17) into Eq. (20), we can obtain an analytical expression of the rectifying factor,

$$R = \frac{\kappa F^2 - \kappa_a S\left[\frac{1}{2},0,0,1\right]}{\kappa F^2 + \kappa_a S\left[\frac{1}{2},0,0,1\right]}. \qquad (21)$$

By this definition, $R = -1$ implies maximal rectification with enhanced transport to the left (left rectification), $R = 0$ indicates no rectification, while $R = 1$ describes maximal rectification with transport to the right (right rectification).

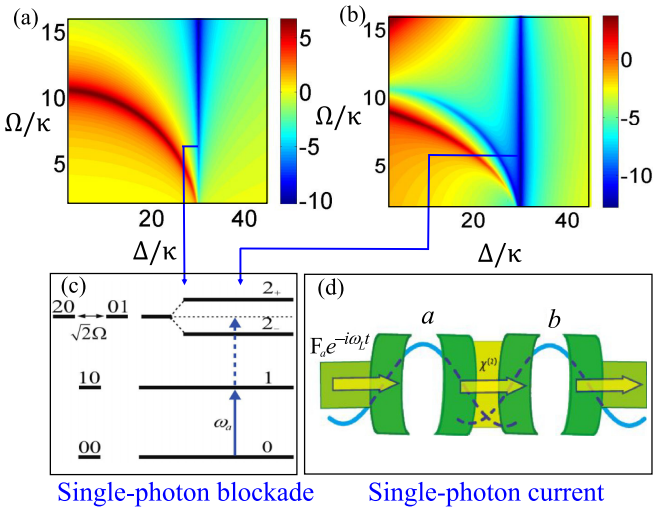

FIG. 3. (Color online) Single-photon rectification in the semiconductor microcavities coupled via χ^2 nonlinearities. The equal-time second-order correlation function when the system is pumped on the cavity a [see analytical expression given by Eq. (17)] (log scale). (a) is for cavity a and (b) is for cavity b. We set $x = \Delta_b + 2\Delta_a$, with detunings given by $\Delta = \Delta_b - 2\Delta_a$ corresponding to $\Delta_a = (x - \Delta)/4$ and $\Delta_b = (x + \Delta)/2$. Parameters chosen are $\kappa_a = 0.1\kappa$, $F = 0.1\kappa$, $x = 30\kappa$. The very narrow region around $\Delta = 30\kappa$, i.e., $\Delta_a \approx 0$, shows the complete single-photon blockade, the corresponding transition is shown in (c), and the single-photon current to right cavity b is illustrated in (d).

In Fig. 3, we plot the second-order correlation function of the left cavity a [see Fig. 3(a)] and right cavity b [see Fig. 3(b)] when the system is pumped on the cavity a. We find that the normalized correlations of $g^{(2)}_j(0) \ll 1$ reach their minimum at $\Delta = 30\kappa$ (namely, $\Delta_a \approx 0$), implying the well-known single-photon blockade. The diagram in Fig. 3(c) illustrates the transition for this blockade.

In Fig. 4, we plot the correlation function of cavity a [see Fig. 4(a)] and cavity b [see Fig. 4(b)] when the system is pumped on the right cavity b. We observe that the minimum of $g^{(2)}_b(0)$ is on an ellipse defined by Eq. (22) and shown in Fig. 4(c). This can be explained as the condition for the two-photon blockade to happen in the system, i.e., two-photon resonance $2\omega_L = \omega_{2\pm}$ follows

$$\Delta^2 + 8\Omega^2 = x^2, \qquad (22)$$

where $x = \Delta_b + 2\Delta_a$ and $\Delta = \Delta_b - 2\Delta_a$. Analogously, the bunching of a pair of photons for the left cavity a takes place due to the extreme antibunching of the right cavity b. Figure 5 shows R, $g^{(2)}$, and N as a function of laser frequency with a fixed Δ in the small Ω/κ limit. We find a local maximum of left rectification in Fig. 5(a) at $x = 30\kappa$ [marked by B in Fig. 5(c)], which corresponds to the antibunching in Fig. 5(b) at the left cavity a. The total photon current $N(k) = N_a(k) + N_b(k)$ overcomes $N(-k)$ in the area around the $x = 30\kappa$; see Fig. 5(c). This can be explained as the single-photon blockade. From Eq. (A4), we find that the single-photon occupation amplitude $\bar{C}_{10}$ is sufficiently larger than that of the multiphoton, e.g., two-photon occupation

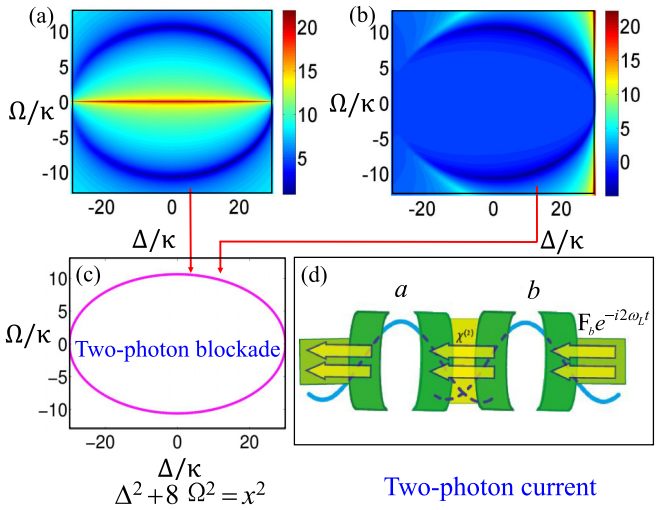

FIG. 4. (Color online) Two-photon rectification in the semiconductor microcavities coupled by χ^2 nonlinearities. The equal-time second-order correlation function [see the analytical expression given by Eq. (15), log scale] of (a) cavity a and (b) cavity b. This figure is plotted with the right cavity b pumped. We set $x = \Delta_b + 2\Delta_a$ with detunings defined by $\Delta = \Delta_b - 2\Delta_a$. Parameters chosen are $\kappa_a = 0.1\kappa$, $F = 0.1\kappa$, and $x = 30\kappa$. At the ellipse, $\Delta^2 + 8\Omega^2 = x^2$, i.e., two-photon resonant transition from $|0\rangle \to |2_\pm\rangle$ when $2\omega_L = \omega_{2\pm}$, the two-photon blockade happens in the semiconductor microcavities. The corresponding transition is illustrated in (c). This causes the two-photon current to the left cavity mode a; see (d). Note that the two-photon current is symmetric for the symmetric coupling Ω in (a) and (b); this is a direct reflection of Eq. (15).

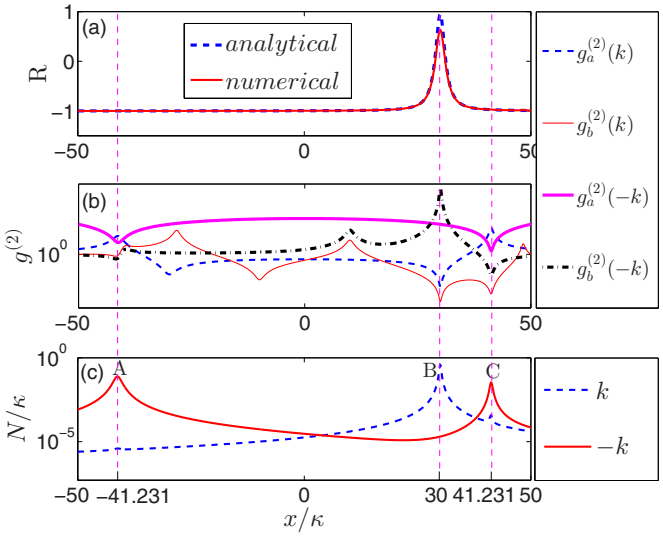

FIG. 5. (Color online) (a) The rectifying factor, correlation function, and total current as a function of frequency of the external laser field x. The blue dashed line and red bold line denote the rectification factor for the analytical expression given by Eq. (21) and the fully numerical simulation in (a), respectively. (b) The equal-time second-order correlation function $g^{(2)}$ [see the analytical expression given by Eqs. (14)–(17)] of the output photon in both directions. (c) The total current, $N(k) = N_a(k) + N_b(k)$ [see the analytical expression given by Eqs. (14)–(17)]. Parameters chosen are $\kappa_a = 0.1\kappa$, $F = 0.1\kappa$, and $\Omega = 10\kappa$. We assume that $\Delta = 30\kappa$ with $\Delta_a = (x - \Delta)/4$ and $\Delta_b = (x + \Delta)/2$.

amplitudes $\bar{C}_{01}$ and $\bar{C}_{20}$ in the limit of weak optical driving, i.e., $|\alpha_j \alpha_k| \ll 1$.

Two maxima of left rectification can be observed at $x = \pm 10\sqrt{17}\kappa \approx \pm 41.231\kappa$ (marked by A and C) from Fig. 5 due to the two-photon blockade at the ellipse given by Eq. (22), which corresponds to the antibunched effect in Fig. 5(b) at the right cavity b with cavity b pumped (denoted by $-k$). The total photon current $N(-k)$ overcomes $N(k)$ in the area around the two points A and C in Fig. 5(c). This observation can be explained by examining Eq. (A1). The contribution of the four-photon terms $\bar{C}_{21}$ and $\bar{C}_{02}$ can be neglected compared to the two-photon occupation amplitude $\bar{C}_{20}$ $\bar{C}_{01}$ when the weak optical driving condition $|\alpha_j \alpha_k| \ll 1$ is satisfied. The one-photon occupation amplitude $\bar{C}_{10}$ and three-photon occupation amplitudes $\bar{C}_{11}$ and $\bar{C}_{30}$ are equal to zero. Therefore, the one- and three-photon processes have no contribution to the two-photon diode.

IV. DELAYED CORRELATION FUNCTION

In addition to the equal-time second-order correlation functions discussed above, quantum signatures can also be manifested in photon intensity correlations with a finite time delay. This motivates us to investigate the dynamical evolution of the second-order time-delayed correlation function. The two-time intensity correlations are defined by [42,54,60]

$$g_a^2(\tau) = g_a^2(\tau = t_1 - t, t \to \infty) = \frac{\langle \hat{a}^\dagger(t)\hat{a}^\dagger(t_1)\hat{a}(t_1)\hat{a}(t)\rangle}{\langle \hat{a}^\dagger(t)\hat{a}(t)\rangle^2}. \tag{23}$$

Rewriting this correlation in terms of a classical light photon intensity I, $g^2(\tau) = \langle I(\tau)I(0)\rangle\langle I\rangle^2$, and using the Schwarz inequality, we obtain the inequality [36,57]

$$g^2(\tau) \leqslant g^2(0). \tag{24}$$

Similar to the inequality $g^{(2)}(0) > 1$ at zero time delay, violation of the inequality at finite time delay is a signature of quantum nature. We calculate the delayed second-order correlation functions for both the left cavity a and right cavity b when the system is pumped on the left cavity a.

The correlation functions $g_a^{(2)}(\tau)$ and $g_b^{(2)}(\tau)$ are shown in Fig. 6 for two strengths of the driving F. We can understand the finite time-delayed intensity correlations in terms of the simple eight-level model discussed in the previous section. For this purpose, we rewrite Eq. (23) as

$$g_a^2(t_1 - t) = \frac{\mathrm{Tr}_S \mathrm{Tr}_E[\hat{a}^\dagger \hat{a} U^\dagger(t - t_1)\hat{a}\rho_{tot}(t)\hat{a}^\dagger U(t - t_1)]}{\langle \hat{a}^\dagger(t)\hat{a}(t)\rangle^2}, \tag{25}$$

where the unitary evolution operator $U(t) = \exp(-i\hat{H}_T t)$, $\hat{H}_T = \hat{H}_S + \hat{H}_E + \hat{H}_I$, and $\hat{H}_S$ is given by Eq. (6). $\hat{H}_E$ and $\hat{H}_I$ are the Hamiltonians of the environment and the system-environment interaction, respectively. We assume $\tau = t_1 - t$ and $t \to \infty$, when the system density matrix arrives at a steady state ρ_s. Applying the Born approximation, we have

$$g_a^2(\tau) = \frac{\mathrm{Tr}_S \mathrm{Tr}_E[\hat{a}^\dagger \hat{a} U(\tau)\hat{a}\rho_s \hat{a}^\dagger \otimes \rho_E U^\dagger(\tau)]}{\bar{n}_a^2}. \tag{26}$$

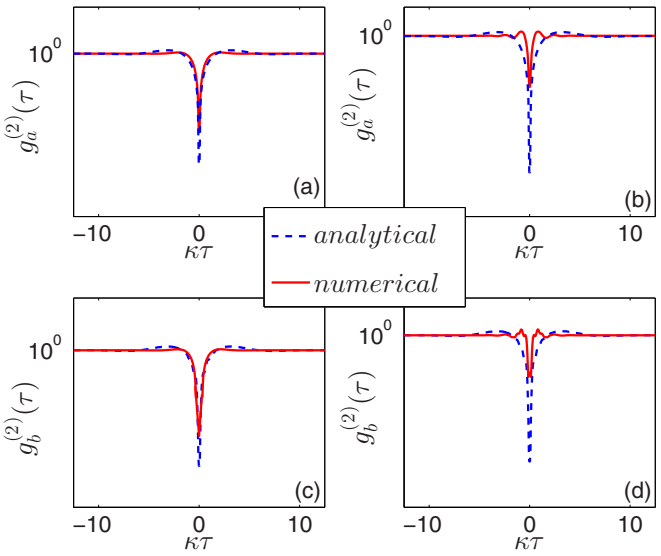

FIG. 6. (Color online) Finite temporal evolution of the second-order correlation function for selected driving strength F with cavity a being pumped. The blue dashed line and red bold line denote the analytical expression [given by Eqs. (30) and (31)] and the exact numerical simulation, respectively. Parameters chosen are $\kappa_a = 1.6\kappa$, $F = 0.72\kappa$, $\Omega = 10\kappa$, $\Delta_a = 0.48\kappa$, and $\Delta_b = 0.4\kappa$ for (a) and (c), and $F = 2\kappa$ for (b) and (d).

A simple calculation follows,

$$g_a^2(\tau) = \mathrm{Tr}_S[\hat{A}^\dagger \hat{A} \rho_{\mathrm{new}}(\tau)], \tag{27}$$

where

$$\rho_{\mathrm{new}}(\tau) = \mathrm{Tr}_E[U(\tau)\rho_{\mathrm{new}}(0) \otimes \rho_E U^\dagger(\tau)], \tag{28}$$

where the new initial state is defined by $\rho_{\mathrm{new}}(0) = \hat{a}\rho_s\hat{a}^\dagger$ and $\hat{A} = \hat{a}/\bar{n}_a$. From Eq. (27), we can find that the finite time-delayed second-order correlation function can be thought of as an expectation value of the effective photon number $\hat{A}^\dagger\hat{A}$ with a new density matrix given by Eq. (28). Note that the new dynamical equation is the same as Eq. (8), i.e., $\dot{\rho}_{\mathrm{new}}(t) \equiv \dot{\rho}(t)$, except that the new initial condition $\rho(0)$ is replaced by $\rho_{\mathrm{new}}(0)$.

Writing the system steady state as $\rho_s = |\bar{\Phi}\rangle\langle\bar{\Phi}|$ and the new time-evolved density matrix as $\rho_{\mathrm{new}}(t) = |\Phi_{\mathrm{new}}(t)\rangle\langle\Phi_{\mathrm{new}}(t)|$, we find $|\dot{\Phi}_{\mathrm{new}}(t)\rangle \equiv |\dot{\Phi}(t)\rangle$ satisfying Eq. (16) within the non-Hermitian Hamiltonian approximation. Therefore, the time-delayed correlation function can be calculated by introducing a new initial state,

$$|\Phi_{\mathrm{new}}(0)\rangle = \hat{a}|\bar{\Phi}\rangle, \tag{29}$$

with $|\bar{\Phi}\rangle$ given by Eq. (16) (see Appendix B). With this initial state, we have the time-delayed correlation function,

$$g_a^2(\tau) = \frac{|C_{10}(\tau)|^2}{|\bar{C}_{10}|^4}, \tag{30}$$

for the left cavity a, while for the right cavity b,

$$g_b^2(\tau) = \frac{|C_{01}(\tau)|^2}{|\bar{C}_{01}|^4}. \tag{31}$$

We note that the non-Hermitian Hamiltonian approximation is a good approximation when

$$\Omega^2 \gg \kappa_a \kappa F. \tag{32}$$

We find from Fig. 6 that when the strong-coupling conditions (32) are satisfied [see Figs. 6(a) and 6(c)] and cavity a is pumped, the finite time-delayed second-order correlation functions given by the analytical expression of Eqs. (30) and (31) are in good agreement with those given by numerical simulations. When the driving strength is strong (32) [see Figs. 6(b) and 6(d)], the analytical expression given by Eqs. (30) and (31) deviates from the numerical simulations. In addition, from Fig. 6, we can observe that the $g_a^{(2)}(\tau)$ and $g_b^{(2)}(\tau)$ increase above their initial value at finite time delay. This is a violation of the inequality in Eq. (24), indicating that photons emitted at different times prefer to stay together. See the red bold line around $\tau \approx \pm 0.827/\kappa$, in Figs. 6(b) and 6(d).

This indicates that two subsequent emissions are suppressed in a single-photon diode, leading to dynamical antibunching both for zero and finite time delays. Hence our proposal provides us with insight into the necessary time delay in a single-photon diode in the semiconductor microcavities coupled via $\chi^{(2)}$ nonlinearities.

V. EXPERIMENTAL REALIZATION

Up to now, based on the model in Eq. (8), we have presented a theoretical proposal for the quantum optical diode and have studied the physics behind the scheme. In the following, we evaluate the actual experimental possibilities to get the proposed optical diode. From the discussion, we find that the possibility to realize such a diode mainly depends on the ratio Ω/κ and the resonators quality factor $Q = \omega/\kappa$. So, we will extensively focus on the parameters Ω and Q.

To simplify the calculation, we assume that the two modes (mode a and mode b) are totally overlapped. This assumption of course increases the coupling constant Ω beyond reality, but it helps to get more insight into the physics of the scheme. On the other side, our proposal works based on the model given by Eq. (8), which does not restrict the two spatially separated modes. With this assumption, we reduce Eq. (4) to

$$\Omega = \tilde{\chi}^{(2)} \sqrt{\frac{\hbar}{\varepsilon_0 V_{\mathrm{eff}}}} \left(\frac{\omega_a}{\varepsilon_r}\right)^{1.5}, \tag{33}$$

where we have chosen $\omega_b = 2\omega_a$, and $\phi_a(\mathbf{r}) = \phi_b(\mathbf{r}) = \phi(\mathbf{r})$. In this situation, an effective mode volume for the scalar field profile can be defined in Eq. (33) as $V_{\mathrm{eff}}^{-1/2} = \int \phi^3(\mathbf{r}) d^3\mathbf{r}$. Furthermore, we assume the real part of $\chi^{(2)}$ constant, denoted by $\tilde{\chi}^{(2)}$. This can be achieved in photonic crystal resonators at near infrared wavelengths [61]. Taking a simple normalized mode profile $\phi(r) = (2/\pi a_x a_y d)^{1/2} \exp(-x^2/2a_x^2 - y^2/2a_y^2)\cos[(\pi/d)z]$ into account, we have $V_{\mathrm{eff}} = 4\pi a_x a_y d/3$.

For dielectric photonic microcavities [62], we may take $a_x = \lambda/(2\sqrt{\varepsilon_r})$, $a_y = d = a_x/3$, $\varepsilon_r = 2$. Using these parameters and taking $\lambda = 1.5\ \mu$m, we find $V_{\mathrm{eff}} = 0.07\ \mu\mathrm{m}^3$. The value of $\chi^{(2)}$ in GaAs is 200 pm/V at wavelengths of around 1.5 μm [63]. Collecting all these together, we get a realistic order of magnitude for the coupling constant in Eq. (4) as $\hbar\Omega \sim 27\ \mu$eV, which is sufficient to meet the requirement of

the quantum optical diode operation. As to the cavity loss rate, with state-of-the-art capabilities, the regime of quantum optical diode operation can be achieved in standard III-V semiconductor microresonators with quality factors on the order of 10^5, so $Q_a = 5Q_b = 7\times 10^5$ [64] is reasonable. This leads to $\hbar\kappa_b = 10\hbar\kappa_a \sim 2.3$ μeV, which is about the ratio used in our simulations, e.g., $\Omega/\kappa \equiv \Omega/\kappa_b \sim 10$. Hence the proposal is realizable within recent technologies.

VI. CONCLUSION

In summary, we have presented a scheme for creating an optical diode, in which the diode is composed of two microcavities coupled via $\chi^{(2)}$ nonlinearities. A master equation to describe such a system is given. By solving this master equation, one- and two-photon blockades are predicted. By the use of this photon blockade, we design an optical diode, which has the ability to combine photon rectification and one-photon to two-photon conversion. To characterize the rectification, we calculated both analytically and numerically the two-order correlation function and the rectifying factor in the weakly driven limit. The numerical simulation and analytical expression agree well with each other. The proposal is within reach by current technologies, especially in the state-of-the-art III-V semiconductor microcavities. The ultimate goal of this research would be to achieve complete control over quantum transport, which includes perfect quantum state transfer and rectification. We believe this type of quantum device might become a key element in most integrated circuits for quantum information science.

ACKNOWLEDGMENTS

We would like to thank Professor W. T. M. Irvine for helpful discussions. This work is supported by the NSF of China under Grant No. 11175032.

APPENDIX A: ANALYTICAL EXPRESSION

In this appendix, we provide the analytical expression used to calculate zero and finite time-delayed second-order correlation functions in the steady state. First, zero time-delayed correlations are calculated by the use of steady-state solutions of Eq. (13). We set the time derivatives to zero and solve the equations iteratively, order by order, in the weak driving limit. With the right microcavity b being pumped, simple calculation yields

$$\begin{aligned}
\bar{C}_{00} &= 1,\\
\bar{C}_{10} &= C_{11} = C_{30} = 0,\\
\bar{C}_{20} &= \frac{\alpha_a x_b}{\sqrt{2}(1-x_a x_b)},\\
\bar{C}_{01} &= -\frac{\alpha_b}{1-x_a x_b},\\
\bar{C}_{21} &= \frac{-\alpha_a\alpha_b(2+y)x_b}{\sqrt{2}(2+y-2x_a x_b)(1-x_a x_b)},\\
\bar{C}_{02} &= \frac{\alpha_a\alpha_b(2+y+x_a x_b y)}{\sqrt{2}y(2+y-2x_a x_b)(1-2x_a x_b)},
\end{aligned} \tag{A1}$$

where $\alpha_j = -iF/\delta_j (|\alpha_j|^2$ or $|\alpha_j\alpha_k| \ll 1)$, $x_j = -i\Omega/\delta_j$, and $y = \delta_b/\delta_a$. Using these amplitudes, we can express all equal-time averages. The mean photon number is

$$\bar{n}_a = 2|\bar{C}_{20}|^2, \quad \bar{n}_b = |\bar{C}_{01}|^2, \tag{A2}$$

and the photon-photon correlation functions are

$$g_b^{(2)}(0) = \frac{2|\bar{C}_{02}|^2}{|\bar{C}_{01}|^4}, \quad g_a^{(2)}(0) = \frac{1}{2|\bar{C}_{20}|^2}. \tag{A3}$$

Therefore, Eqs. (14) and (15) can be obtained by substituting Eq. (A1) into Eqs. (A2) and (A3), respectively. Next we calculate these occupation amplitudes for pumping on the left cavity a,

$$\begin{aligned}
\bar{C}_{00} &= 1,\\
\bar{C}_{10} &= -\alpha_a,\\
\bar{C}_{01} &= \frac{\alpha_a\alpha_b x_a}{(x_a x_b - 1)},\\
\bar{C}_{20} &= -\frac{\alpha_a^2}{\sqrt{2}(x_a x_b - 1)},\\
\bar{C}_{30} &= \frac{\alpha_a^2\alpha_b\left(2+3y+y^2+2x_a x_b - 4x_a^2 x_b^2\right)}{\sqrt{6}\eta(x_a x_b - 1)},\\
\bar{C}_{11} &= \frac{-\alpha_a\alpha_b^2 x_a\left(2+3y+y^2-2x_a x_b - 2x_a^2\right)}{\eta(x_a x_b - 1)},\\
\bar{C}_{21} &= \frac{\sqrt{2}\alpha_a^2\alpha_b^2 x_a(1+y)}{\eta(x_a x_b - 1)},\\
\bar{C}_{02} &= \frac{-\sqrt{2}\alpha_a^2\alpha_b^2 x_a x_b(1+y)}{\eta(x_a x_b - 1)},
\end{aligned} \tag{A4}$$

where the coefficient $\eta = (2y^{-1} + 3 + y - 2x_b^2 - 6x_a x_b - 2x_a^2 + 4x_a^2 x_b^2)$. The mean photon numbers and the photon-photon correlation functions are

$$\begin{aligned}
\bar{n}_b &= |\bar{C}_{01}|^2, \quad \bar{n}_a = |\bar{C}_{10}|^2,\\
g_b^{(2)}(0) &= \frac{2|\bar{C}_{02}|^2}{|\bar{C}_{01}|^4}, \quad g_a^{(2)}(0) = \frac{2|\bar{C}_{20}|^2}{|\bar{C}_{10}|^4}.
\end{aligned} \tag{A5}$$

Equation (17) can be obtained by substituting Eq. (A4) into Eqs. (A5).

APPENDIX B: DELAYED CORRELATION FUNCTION

The dynamical evolution of the second-order correlation function can be calculated within the same approach as in Appendix A by the use of Eq. (29) as the initial condition and assuming a pumping is on the left cavity a. Specifically, the unnormalized state after the annihilation of a photon in the left cavity a is $\hat{a}|\bar{\Phi}\rangle = \bar{C}_{10}|00\rangle + \sqrt{2}\bar{C}_{20}|10\rangle$, where we have ignored the high-order terms. With this understanding in mind, Eq. (30) can be obtained by solving the first four equations of Eq. (16) for the amplitudes with the initial condition.

The correlation function of the right cavity b mode $g_b^2(\tau)$ may be calculated similarly. The state after annihilation of a photon in the b mode is $\hat{b}|\bar{\Phi}\rangle = \bar{C}_{01}|00\rangle + \bar{C}_{11}|10\rangle + \bar{C}_{21}|20\rangle + \sqrt{2}\bar{C}_{02}|01\rangle$. Using this as the initial condition, Eq. (31) can be obtained by solving Eq. (16).

[1] B.-W. Li, L. Wang, and G. Casati, Phys. Rev. Lett. **93**, 184301 (2004).
[2] B.-W. Li, J.-H. Lan, and L. Wang, Phys. Rev. Lett. **95**, 104302 (2005).
[3] C. W. Chang, D. Okawa, A. Majumdar, and A. Zettl, Science **314**, 1121 (2006).
[4] W. Kobayashi, Y. Teraoka, and I. Terasaki, Appl. Phys. Lett. **95**, 171905 (2009).
[5] M. Terraneo, M. Peyrard, and G. Casati, Phys. Rev. Lett. **88**, 094302 (2002).
[6] R. Scheibner, M. König, D. Reuter, A. D. Wieck, C. Gould, H. Buhmann, and L. W. Molenkamp, New J. Phys. **10**, 083016 (2008).
[7] V. F. Nesterenko, C. Daraio, E. B. Herbold, and S. Jin, Phys. Rev. Lett. **95**, 158702 (2005).
[8] L. J. Aplet and J. W. Carson, Appl. Opt. **3**, 544 (1964).
[9] P. Yeh, *Optical Waves in Layered Media* (Wiley, New York, 1988).
[10] B. E. A. Saleh and M. C. Teich, *Fundamentals of Photonics*, 2nd ed. (Wiley, New York, 2007).
[11] M. S. Kang, A. Butsch, and P. S. Russell, Nat. Photon. **5**, 549 (2011)
[12] A. Kamal, J. Clarke, and M. H. Devoret, Nat. Phys. **7**, 311 (2011).
[13] L. Fan, J. Wang, L. T. Varghese, H. Shen, B. Niu, Y. Xuan, A. M. Weiner, and M.-H. Qi, Science **335**, 447 (2012).
[14] L. Bi, J. Hu, P. Jiang, D. H. Kim, G. F. Dionne, L. C. Kimerling, and C. A. Ross, Nat. Photon. **5**, 758 (2011).
[15] Z. F. Yu and S. H. Fan, Nat. Photon. **3**, 91 (2009).
[16] A. Alberucci and G. Assanto, Opt. Lett. **33**, 1641 (2008).
[17] F. Biancalana, J. Appl. Phys. **104**, 093113 (2008).
[18] Y. Shen, M. Bradford, and J.-T. Shen, Phys. Rev. Lett. **107**, 173902 (2011).
[19] B. Liang, B. Yuan, and J. C. Cheng, Phys. Rev. Lett. **103**, 104301 (2009).
[20] B. Liang, X.-S. Guo, J. Tu, D. Zhang, and J. C. Cheng, Nat. Mater. **9**, 989 (2010).
[21] D.-W. Wang, H.-T. Zhou, M.-J. Guo, J.-X. Zhang, J. Evers, and S.-Y. Zhu, Phys. Rev. Lett. **110**, 093901 (2013).
[22] C. Flindt, A. S. Sørensen, M. D. Lukin, and J. M. Taylor, Phys. Rev. Lett. **98**, 240501 (2007).
[23] D. Roy, Phys. Rev. B **81**, 155117 (2010).
[24] G. Nikoghosyan and M. Fleischhauer, Phys. Rev. Lett. **103**, 163603 (2009).
[25] J. C. Blakesley, P. See, A. J. Shields, B. E. Kardynał, P. Atkinson, I. Farrer, and D. A. Ritchie, Phys. Rev. Lett. **94**, 067401 (2005).
[26] H. Lira, Z. Yu, S. Fan, and M. Lipson, Phys. Rev. Lett. **109**, 033901 (2012).
[27] J. L. O'Brien, A. Furusawa, and J. Vučković, Nat. Photon. **3**, 687 (2009).
[28] E. Mascarenhas, D. Gerace, D. Valente, S. Montangero, A. Auffèves, and M. F. Santos, Europhys. Lett. **106**, 54003 (2014).
[29] W. T. M. Irvine, K. Hennessy, and D. Bouwmeester, Phys. Rev. Lett. **96**, 057405 (2006).
[30] G. S. Agarwal, Phys. Rev. Lett. **73**, 522 (1994).
[31] I. Carusotto and G. C. La Rocca, Phys. Rev. B **60**, 4907 (1999).
[32] A. Majumdar and D. Gerace, Phys. Rev. B **87**, 235319 (2013).
[33] Y.-C. Liu, Y.-F. Xiao, Y.-L. Chen, X.-C. Yu, and Q.-H. Gong, Phys. Rev. Lett. **111**, 083601 (2013).
[34] L. Tian and H. J. Carmichael, Phys. Rev. A **46**, R6801 (1992).
[35] M. J. Werner and A. Imamolu, Phys. Rev. A **61**, 011801(R) (1999).
[36] R. J. Brecha, P. R. Rice, and M. Xiao, Phys. Rev. A **59**, 2392 (1999).
[37] S. Rebić, S. M. Tan, A. S. Parkins, and D. F. Walls, J. Opt. B **1**, 490 (1999).
[38] S. Rebić, A. S. Parkins, and S. M. Tan, Phys. Rev. A **65**, 063804 (2002).
[39] J. Kim, O. Bensen, H. Kan, and Y. Yamamoto, Nature (London) **397**, 500 (1999).
[40] I. I. Smolyaninov, A. V. Zayats, A. Gungor, and C. C. Davis, Phys. Rev. Lett. **88**, 187402 (2002).
[41] M. Bamba, A. Imamolu, I. Carusotto, and C. Ciuti, Phys. Rev. A **83**, 021802(R) (2011).
[42] T. C. H. Liew and V. Savona, Phys. Rev. Lett. **104**, 183601 (2010).
[43] A. Miranowicz, M. Paprzycka, Y.-X. Liu, J. Bajer, and F. Nori, Phys. Rev. A **87**, 023809 (2013).
[44] P. Rabl, Phys. Rev. Lett. **107**, 063601 (2011).
[45] J.-Q. Liao and C. K. Law, Phys. Rev. A **82**, 053836 (2010).
[46] P. Kómár, S. D. Bennett, K. Stannigel, S. J. M. Habraken, P. Rabl, P. Zoller, and M. D. Lukin, Phys. Rev. A **87**, 013839 (2013).
[47] J.-Q. Liao and F. Nori, Phys. Rev. A **88**, 023853 (2013).
[48] A. J. Hoffman, S. J. Srinivasan, S. Schmidt, L. Spietz, J. Aumentado, H. E. Türeci, and A. A. Houck, Phys. Rev. Lett. **107**, 053602 (2011).
[49] C. Lang, D. Bozyigit, C. Eichler, L. Steffen, J. M. Fink, A. A. Abdumalikov, Jr., M. Baur, S. Filipp, M. P. da Silva, A. Blais, and A. Wallraff, Phys. Rev. Lett. **106**, 243601 (2011).
[50] R. W. Boyd, *Nonlinear Optics* (Academic, New York, 2008).
[51] M. J. Collett and C. W. Gardiner, Phys. Rev. A **30**, 1386 (1984).
[52] C. W. Gardiner and M. J. Collett, Phys. Rev. A **31**, 3761 (1985).
[53] H. Z. Shen, M. Qin, and X. X. Yi, Phys. Rev. A **88**, 033835 (2013).
[54] A. Verger, C. Ciuti, and I. Carusotto, Phys. Rev. B **73**, 193306 (2006).
[55] R. Loudon, *The Quantum Theory of Light* (Oxford University Press, Oxford, 2003).
[56] S. Ferretti and D. Gerace, Phys. Rev. B **85**, 033303 (2012).
[57] H. J. Carmichael, R. J. Brecha, and P. R. Rice, Opt. Commun. **82**, 73 (1991).
[58] S. Weis, R. Rivi'ere, S. Del eglise, E. Gavartin, O. Arcizet, A. Schliesser, and T. J. Kippenberg, Science **330**, 1520 (2010).
[59] M. D. Lukin, Rev. Mod. Phys. **75**, 457 (2003).
[60] S. Ferretti, L. C. Andreani, H. E. Türeci, and D. Gerace, Phys. Rev. A **82**, 013841 (2010).
[61] M. Notomi, Rep. Prog. Phys. **73**, 096501 (2010).
[62] J. T. Robinson, C. Manolatou, L. Chen, and M. Lipson, Phys. Rev. Lett. **95**, 143901 (2005).
[63] S. Bergfeld and W. Daum, Phys. Rev. Lett. **90**, 036801 (2003).
[64] S. Combrié, A. De Rossi, N.-Q.-V. Tran, and H. Benisty, Opt. Lett. **33**, 1908 (2008).